THE JOURNAL OF BIOLOGICAL CHEMISTRY VOL. 288, NO. 33, pp. 23666–23674, August 16, 2013

Phosphatidylglycerol Directs Binding and Inhibitory Action of EIIA^{Glc} Protein on the Maltose Transporter*

Received for publication, May 29, 2013, and in revised form, June 26, 2013 Published, JBC Papers in Press, July 2, 2013, DOI 10.1074/jbc.M113.489567

Huan Bao and Franck Duong[1]

From the Department of Biochemistry and Molecular Biology, Life Sciences Institute, Faculty of Medicine, University of British Columbia, Vancouver, British Columbia V6T1Z3, Canada

Background: The protein EIIA^{Glc} inhibits maltose transport.
Results: Anionic lipids and N-terminal tail direct the positioning of EIIA^{Glc} onto the MalK dimer to inhibit cleavage of ATP.
Conclusion: A mechanism of inhibition of maltose transport by EIIA^{Glc} is presented.
Significance: The study highlights the importance of membrane lipids for the correct positioning of EIIA^{Glc} on the transporter.

The signal-transducing protein EIIA^{Glc} belongs to the phosphoenolpyruvate carbohydrate phosphotransferase system. In its dephosphorylated state, EIIA^{Glc} is a negative regulator for several permeases, including the maltose transporter MalFGK$_2$. How EIIA^{Glc} is targeted to the membrane, how it interacts with the transporter, and how it inhibits sugar uptake remain obscure. We show here that acidic phospholipids together with the N-terminal tail of EIIA^{Glc} are essential for the high affinity binding of the protein to the transporter. Using protein docking prediction and chemical cross-linking, we demonstrate that EIIA^{Glc} binds to the MalK dimer, interacting with both the nucleotide-binding and the C-terminal regulatory domains. Dissection of the ATPase cycle reveals that EIIA^{Glc} does not affect the binding of ATP but rather inhibits the capacity of MalK to cleave ATP. We propose a mechanism of maltose transport inhibition by this central amphitropic regulatory protein.

Bacteria selectively metabolize certain sugars through a mechanism termed carbon catabolite repression (1). In enteric bacteria, the phosphoenolpyruvate carbohydrate phosphotransferase system regulates the selective utilization of these carbon sources (2). The phosphotransferase system consists of a sugar transporter and a phosphorylation system that is composed of at least three distinct components: the enzyme EI, the phosphocarrier protein HPr, and several sugar-specific enzymes called EII. Transport across the membrane of a preferred sugar leads to the transfer of a phosphoryl group from phosphoenolpyruvate to the different EII proteins, whose action is to reduce utilization of nonpreferred carbon sources (3). Among the different EII proteins, the role of the glucose-specific EIIA^{Glc} [2] has been particularly well studied. The dephosphorylated form of EIIA^{Glc}, present during glucose transport, is responsible for the allosteric inhibition of several permeases and kinases involved in the import of maltose, lactose, melibiose, and glycerol (2).

The astonishing capacity of EIIA^{Glc} to regulate the activity of numerous enzymes, located both in the cytosol and within the membrane, has raised some interesting questions regarding the mechanism of recognition and interaction (3–7). On its own, the protein consists of an unstructured N-terminal tail (residues 1–18) attached to a globular core (residue 19–168) made by an antiparallel β-sheet sandwich (8). Structural analyses of EIIA^{Glc} in complex with some of its cytosolic effectors, such as the phosphocarrier protein HPr, the glycerol kinase, and the subunit EIIB^{Glc}, have revealed a common binding surface on the globular core of EIIA^{Glc} (5–7). For the membrane permease, a limited number of studies based on peptide mapping and site-directed mutagenesis concluded that the same binding surface is also involved in the recognition of the maltose and lactose permeases (9, 10). However, the affinity of EIIA^{Glc} for these permeases is weak, and the modality of inhibition remains obscure, in part due to the difficulty of isolating complexes suitable for structural analysis. Interestingly, it was reported that the N-terminal tail of EIIA^{Glc} is essential for the inhibition of the lactose and maltose permeases, but not for inhibition of cytosolic proteins such as HPr (8, 9, 11, 12). It was also found that a synthetic peptide corresponding to the N-terminal tail of EIIA^{Glc} could adopt an amphipathic helical structure in the presence of phosphatidylglycerol (PG) lipids (8, 13). Together, these earlier observations hint at a possible mechanism to increase the binding of EIIA^{Glc} to the membrane permeases.

In this work, we investigate the association of EIIA^{Glc} with the maltose transporter MalFGK$_2$. The transporter consists of two membrane-integral subunits, MalF and MalG, and two copies of the ATPase subunit, MalK. We show that phosphatidylglycerol and the N-terminal amphipathic tail of EIIA^{Glc} are essential for the inhibition of the ATPase activity of the transporter. Using site-directed cross-linking experiments, we map the interaction of EIIA^{Glc} to the nucleotide-binding domain

* This work was supported by an infrastructure grant from the Canadian Foundation for Innovation and operating grants from the Natural Sciences and Engineering Research Council of Canada (NSERC).

[1] The recipient of a Canada Research Chair II award. To whom correspondence should be addressed: Dept. of Biochemistry and Molecular Biology, Life Sciences Institute, Faculty of Medicine, University of British Columbia, 2350 Health Sciences Mall, Vancouver, British Columbia V6T1Z3, Canada. Tel.: 604-822-5975; Fax: 604-822-522; E-mail: fduong@mail.ubc.ca.

[2] The abbreviations used are: EIIA^{Glc}, glucose-specific EIIA; SPDP, succinimidyl 3-(2-pyridyldithio)-propionate; TNP-ATP, 2′(3′)-O-(2,4,6-trinitrophenyl) adenosine 5′-triphosphate; PG, phosphatidylglycerol; PC, phosphatidylcholine; DOPG, dioleoylphosphatidylglycerol; DOPC, dioleoylphosphatidylcholine; MTS-3-MTS, 1,3-propanediyl bismethanethiosulfonate; NBD, nucleotide-binding domain.

and the C-terminal regulatory domain of the MalK dimer. Analysis of the ATPase cycle under single and multiple turnover conditions shows that EIIA^{Glc} does not change the affinity of MalK for nucleotide but instead inhibits its capacity to cleave ATP.

EXPERIMENTAL PROCEDURES

Reagents—*N*-Dodecyl-β-D-maltoside was purchased from Anatrace. All lipids were obtained from Avanti Polar Lipids. Bio-Beads were purchased from Bio-Rad. Ni^{2+}-nitrilotriacetic acid chelating Sepharose, Superose 6 10/300 GL, Superdex 200 10/300 GL, and Sephadex G-25 were obtained from GE Healthcare. Cross-linkers disuccinimidyl suberate and succinimidyl 3-(2-pyridyldithio)-propionate (SPDP) were from Thermo Scientific, and 1,3-propanediyl bismethanethiosulfonate (MTS-3-MTS) was from Toronto Research Chemicals. Radiolabeled nucleotides [α-^{32}P]ATP (25 Ci/mmol) and [γ-^{32}P]ATP (800 Ci/mmol) were purchased from MP Biomedicals. All other chemicals, including TNP-ATP and polyethylenimine cellulose TLC plates, were obtained from Sigma.

Protein Purification—The production and purification of MalE and His-tagged MalFGK$_2$ were as described previously (14). Mutations were introduced by site-directed PCR mutagenesis and verified by DNA sequencing. The chromosomal gene *crr* (encoding for EIIA^{Glc}) was cloned into pBAD33 with a His$_6$ tag sequence introduced at the 3′ end of the gene, yielding plasmid p33-EIIA$_{his}$. Overproduction of EIIA^{Glc} was achieved in *Escherichia coli* strain BL21 grown in 6 liters of M9 medium supplemented with chloramphenicol (50 μg/ml) and glucose (0.8%). At A_{600} ~0.5, EIIA^{Glc} synthesis was induced with 0.2% arabinose. After 3 h, cells were collected in TSG buffer (50 mM Tris-HCl, pH 8; 100 mM NaCl; 10% glycerol) containing 0.01% PMSF and lysed through a French press (8,000 p.s.i., twice). After ultracentrifugation (100,000 × *g*, 1 h, 4 °C), the supernatant was applied onto a Ni^{2+}-nitrilotriacetic acid-Sepharose column (5 ml) equilibrated in TSG buffer. The washing step was in TSG buffer plus 30 mM imidazole (10 column volumes), and the elution was across a gradient of TSG buffer plus 0–600 mM imidazole. The eluted EIIA^{Glc} protein was further purified on a Superdex 200 GL 10/300 in TSG buffer. Purified EIIA^{Glc} and EIIA^{Glc}Δ1–18 were homogeneous, forming a single elution peak in size-exclusion chromatography and migrating at their expected position on SDS-PAGE analysis (~19 and ~17 kDa, respectively).

Nanodisc Preparation—The reconstitution of the maltose transporter in nanodiscs, at low and high lipid ratio, has been previously described in detail (14–16). Briefly, the MalFGK$_2$ complex, the membrane scaffold protein (MSP1D1), and the indicated lipids were mixed together at a ratio of 1:3:60 or 1:3:400 (MalFGK$_2$:MSP1D1:lipid) in TSG buffer containing 0.04% *N*-dodecyl-β-D-maltoside. The detergent molecules were removed by incubation with Bio-Beads (⅓ volume) overnight at 4 °C under gentle shaking. The Bio-Beads were removed by sedimentation, and the nanodisc particles were purified from aggregates on Superose 6 10/300 GL equilibrated in TSG buffer. The nanodisc preparation was stored at −80 °C. The incorporation of MalFGK$_2$ into proteoliposomes was performed as described previously (14, 15).

Cross-linking Reactions—The cross-linking reactions using disuccinimidyl suberate and SPDP were performed in HM buffer (50 mM K-HEPES, pH 7.5; 10 mM $MgCl_2$). The cross-linking reactions using MTS-3-MTS were in TM buffer (50 mM Tris-HCl, pH 8.0; 10 mM $MgCl_2$). The MalFGK$_2$ proteoliposomes (2 μM) and EIIA^{Glc} (10 μM) were mixed together and incubated with 100 μM of the indicated cross-linker for 20 min at room temperature. The reactions were stopped with Tris-HCl (100 mM) or *N*-ethylmaleimide (5 mM) where appropriate. Proteins were dissolved in sample buffer and analyzed by SDS-PAGE and Western blotting against MalK (17).

Fluorescence Spectroscopy—The fluorescence measurements were performed at 25 °C using a Cary Eclipse spectrofluorometer. Excitation and emission wavelengths were 405 and 535 nm, respectively (10-nm slit widths). To determine the binding affinity of TNP-ATP, the lipid-rich MalFGK$_2$ nanodiscs (2 μM) were incubated with TNP-ATP, and the fluorescence signal was allowed to equilibrate for 3 min. For each amount of TNP-ATP employed, the fluorescence measured in the presence of MalFGK$_2$ nanodiscs was subtracted from that measured in the absence of MalFGK$_2$ nanodiscs, yielding the subtracted fluorescence value (F_s). The data were then plotted as a function of TNP-ATP concentration (L) and fit to Equation 1,

$$F_s = F_{max} \times \frac{[L]}{[L] + K_d} \quad \text{(Eq. 1)}$$

where F_{max} is the maximal subtracted fluorescence at saturating amount of TNP-ATP, and K_d is the equilibrium dissociation constant of TNP-ATP for MalFGK$_2$. For measuring the apparent affinity of ATP for MalFGK$_2$, the lipid-rich MalFGK$_2$ nanodiscs (2 μM) were mixed with TNP-ATP (80 μM) for 5 min at room temperature and then titrated with the indicated amount of ATP. The fluorescence data were fit to Equation 2,

$$F_s = F_0 \times \frac{K_{i,app}}{[I] + K_{i,app}} + F_1 \times \frac{[I]}{[I] + K_{i,app}} \quad \text{(Eq. 2)}$$

in which F_0 is the subtracted fluorescence in the absence of ATP, F_1 is the subtracted fluorescence in the presence of saturating amount of ATP, $[I]$ is the ATP concentration, and $K_{i,app}$ is the apparent inhibition constant of ATP at the specified amount of TNP-ATP. The $K_{d,app}$ of ATP for MalFGK$_2$ is calculated from $K_{i,app}$ by Equation 3,

$$K_{i,app} = K_{d,app} \times \left(1 + \frac{[L]}{K_d}\right) \quad \text{(Eq. 3)}$$

in which $[L]$ is the TNP-ATP concentration, and K_d is the dissociation constant of TNP-ATP for MalFGK$_2$.

Thin-layer Chromatography (TLC)—ATPase hydrolysis assays were performed in TM buffer at room temperature with the indicated amount of [α-^{32}P]ATP or [γ-^{32}P]ATP. Reactions were either stopped at 4 °C by the addition of ice-cold EDTA (20 mM) and proteinase K (1 mg/ml) or subjected to centrifugal gel filtration using a desalting G25 spin column at 4 °C in TM buffer. The eluted protein samples (0.5 μl) were loaded at the bottom of a 10-cm-long PEI cellulose plate. The TLC was developed for 45 min in 0.3 M potassium phosphate, pH 3.4. The

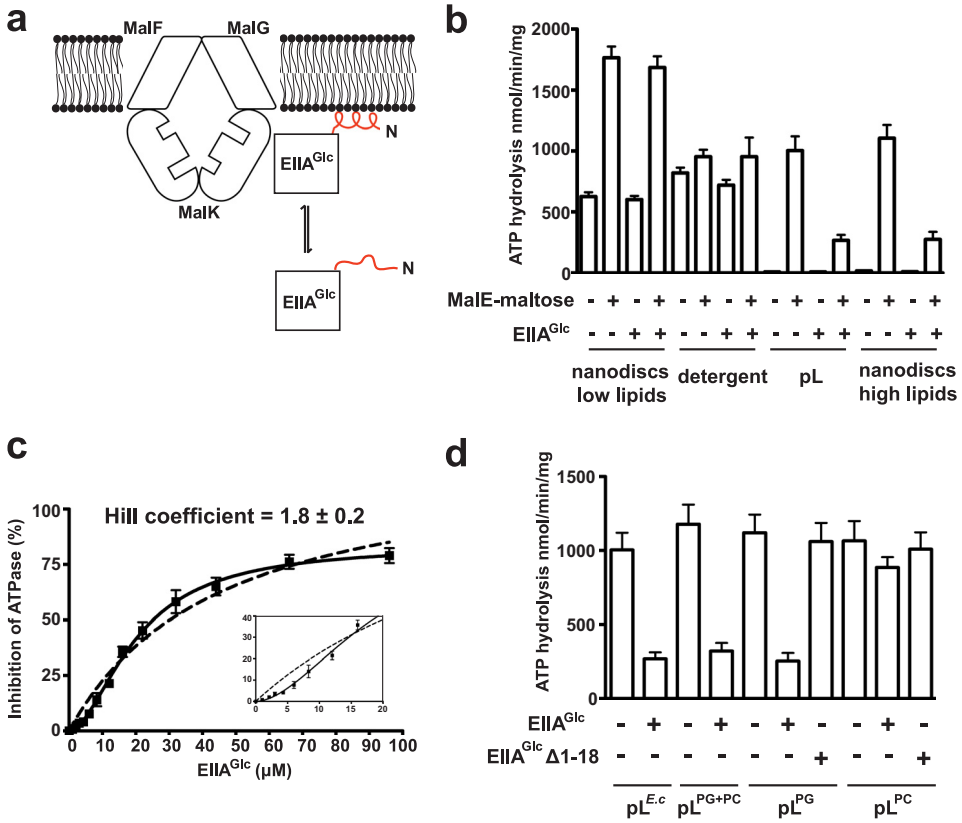

FIGURE 1. **The activity of EIIA^{Glc} depends on intact N-terminal α-helix and PG lipids.** *a*, working model for EIIA^{Glc} binding to the membrane. The N-terminal amphipathic α-helix (residues 1–18) of EIIA^{Glc} is colored in *red*. *b*, the maltose transporter was reconstituted in proteoliposomes (*pL*) and lipid-rich nanodiscs (high lipid ratio) using total *E. coli* lipids. The ATPase activity of the transporter (2 μM each) was determined at 37 °C in the presence of EIIA^{Glc} (96 μM), MalE (10 μM), and maltose (1 mM), as indicated. The activity of the maltose transporter in detergent solution or reconstituted in nanodisc at low lipid ratio is presented for comparison. Three independent experiments were analyzed (mean and S.D.). *c*, the inhibition of MalFGK$_2$ ATPase activity is cooperative. The maltose transporter was reconstituted in proteoliposomes (2 μM) made with DOPG. ATPase activities were determined in the presence of MalE (10 μM) and maltose (1 mM). Three independent experiments were analyzed (mean and S.D.). The data (*black squares*) were fit to a one-site binding equation (*dashed line*) or to its expanded version, which includes a term for the Hill coefficient (*solid line*). The *inset* shows a magnification of the data up to 20 μM EIIA^{Glc}. *d*, the maltose transporter was reconstituted in proteoliposomes (2 μM MalFGK$_2$) made of *E. coli* total lipids (*pL$^{E.c}$*), DOPG (*pL^{PG}*), DOPC (*pL^{PC}*), or a mixture of DOPC and DOPG (70 and 30%, respectively; *pL^{PG+PC}*). The transporter ATPase activity in the presence of MalE (10 μM) and maltose (1 mM) was determined at 37 °C, supplemented with EIIA^{Glc} (96 μM) and EIIA^{Glc}Δ1–18 (98 μM), as indicated. Three independent experiments were analyzed (mean and S.D.).

radioactive spots were revealed by a PhosphorImager scanner, and their intensity was quantified using ImageQuant (GE Healthcare).

Other Methods—The rate of ATP hydrolysis (production of P_i) was determined by the malachite green method (16). For the co-sedimentation assays, the MalFGK$_2$ proteoliposomes (5 μM) and the indicated amount of EIIA^{Glc} were incubated in TM buffer for 5 min at room temperature. The samples were diluted 25-fold into Tris-HCl (20 mM, pH 8), collected by ultracentrifugation (100,000 × *g*, 1 h), and resuspended in Tris-HCl (20 mM, pH 8) followed by SDS-PAGE analysis. The automatic protein docking analysis was performed on the ClusPro 2.0 Web server (18), using the crystallography structures of EIIA^{Glc} (Protein Data Bank (PDB) 1F3G) and MalFGK$_2$ (PDB 3FH6 and 2R6G) (4, 19, 20).

RESULTS

The Inhibition by EIIA^{Glc} Depends on the N-terminal Tail and PG Lipids—EIIA^{Glc} inhibits the ATPase activity of the maltose transporter reconstituted in proteoliposomes by ~4-fold, as reported previously (9) (Fig. 1*b*). We show here that the ATPase activity of the transporter is virtually unaffected by EIIA^{Glc} when MalFGK$_2$ is maintained in detergent solution or reconstituted in nanodiscs at a low lipid ratio (Fig. 1*b*). These last observations raise the possibility that membrane lipids are necessary for inhibition. Accordingly, an ~4-fold inhibition similar to that seen in proteoliposomes was obtained when the transporter was reconstituted in lipid-rich nanodiscs (Fig. 1*b*). Significantly, the inhibition of MalFGK$_2$ ATPase showed a cooperative dependence on EIIA^{Glc} concentration, with a Hill coefficient of 1.8 (Fig. 1*c*). This last result strongly suggests a 2:1 stoichiometry of interaction between EIIA^{Glc} and MalFGK$_2$.

Because a peptide corresponding to the N-terminal tail of EIIA^{Glc} (residues 1–18) possesses affinity for phosphatidylglycerol (8), we hypothesized that the inhibition of the maltose transporter in proteoliposomes also depends on the presence of the lipid in the membrane or in the disc. EIIA^{Glc} was therefore incubated with the transporter reconstituted in proteoliposomes made with DOPG lipids, DOPC lipids, or a mixture of DOPC (70%) and DOPG (30%). The results only showed a strong inhibition of the MalK ATPase activity when DOPG was present in the membrane (~75% reduction, Fig. 1*d*). The transporter ATPase activity was barely reduced when the trans-

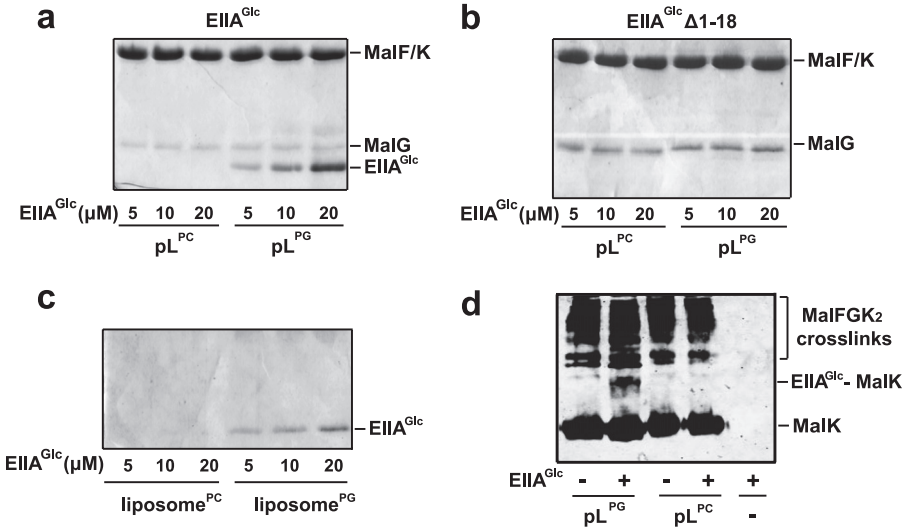

FIGURE 2. **PG lipids control for the binding of EIIA^{Glc} to MalFGK$_2$.** *a*, the transporter reconstituted in proteoliposomes (*pL*) with DOPC (*pL^{PC}*) or DOPG (*pL^{PG}*) lipids, was incubated at room temperature for 5 min with the indicated concentration of EIIA^{Glc}. The proteoliposomes were isolated by ultracentrifugation, and the amount of EIIA^{Glc} bound to MalFGK$_2$ was visualized by SDS-PAGE and Coomassie Blue staining of the gel. *b*, same as *a* but using EIIA^{Glc}Δ1–18. The protein does not co-sediment and therefore does not appear on the SDS-PAGE analysis. *c*, same as *a* but using liposomes devoid of MalFGK$_2$. *d*, the proteoliposomes in *a* were incubated with EIIA^{Glc} (10 μM) and the amine-reactive cross-linker disuccinimidyl suberate (100 μM) for 20 min at room temperature. A control experiment with EIIA^{Glc} alone was performed in parallel (*right lane*). The reactions were stopped with Tris-HCl (100 mM, pH 8). The cross-link products were identified by Western blot using antibodies against MalK. The bands of high molecular weight represent cross-links between MalK and MalFG. An *arrow* indicates the cross-link between MalK and EIIA^{Glc}.

porter was reconstituted with only DOPC lipids (~15% reduction, Fig. 1*d*). To show that the N-terminal tail of EIIA^{Glc} is necessary for inhibition, we employed the mutant EIIA^{Glc} Δ1–18 (Fig. 1*d*). As expected, this mutant protein was unable to inhibit the transporter ATPase activity (less than ~10% reduction).

PG Lipids Are Necessary for the Binding of EIIA^{Glc} to MalFGK$_2$—We employed co-sedimentation assays to monitor the binding of EIIA^{Glc} to MalFGK$_2$. The results show that sedimentation of EIIA^{Glc} occurs only when the MalFGK$_2$ proteoliposomes were made with DOPG lipids. Very little co-sedimentation of EIIA^{Glc} occurred with proteoliposomes made with DOPC (Fig. 2*a*). The sedimentation of EIIA^{Glc} was also reduced to background level when the N-terminal amphipathic helix of EIIA^{Glc} was deleted (Fig. 2*b*). We note that a significant level of binding of EIIA^{Glc} occurs at the surface of the liposomes made with DOPG lipids (Fig. 2*c*). Thus, to demonstrate that EIIA^{Glc} binds to MalFGK$_2$ and not merely to acidic lipids, we employed the amine reactive homobifunctional cross-linker disuccinimidyl suberate. In that case, a prominent cross-link was formed between MalK and EIIA^{Glc}, but only when the proteoliposomes contained DOPG lipids (Fig. 2*d*). Together, these results demonstrate that phosphatidyl glycerol lipids direct the binding of EIIA^{Glc} to the maltose transporter. The binding depends on the N-terminal amphipathic tail of EIIA^{Glc}.

Identification of the Binding Interface between EIIA^{Glc} and MalK—First we employed a molecular modeling approach to identify the potential binding interface between EIIA^{Glc} and MalFGK$_2$. The structure of EIIA^{Glc} (PDB 1F3G) was docked onto the crystal structure of the maltose transporter (PDB 2R6G and 3FH6) using the protein-protein docking server ClusPro (18). This protein docking algorithm uses the fast Fourier transform correlation approach combined with an automatic clustering method to propose interactive surfaces with favorable free energies (18). From the different models proposed (data not shown), we retained the models where EIIA^{Glc} is interacting with the MalK part of the transporter (Fig. 3). Indeed, the mutations that render the transporter resistant to the inhibitory action of EIIA^{Glc} are located in the nucleotide-binding domain (NBD) and the C-terminal domain of the MalK ATPase unit (21–23). It was not possible to determine the stoichiometry of EIIA^{Glc} binding using this automatic docking analysis because the computer program uses a 1:1 mode of interaction. However, because MalK is a symmetric dimer, it can be deduced that two binding sites for EIIA^{Glc} exist on the maltose transporter, in agreement with the Hill coefficient determined above (Fig. 1*c*).

Next, based on the proposed models, we introduced a series of unique cysteine residues into the NBD and C-terminal domain of MalK (Fig. 4). The protein complexes were purified, reconstituted into proteoliposomes with DOPG lipids, and incubated with EIIA^{Glc} in the presence of an amine-to-sulfhydryl cross-linking reagent (SPDP; spacer arm ~7 Å). The protein cross-links were detected by nonreducing SDS-PAGE and immunoblot against MalK. The cysteine positions that formed a covalent bond with EIIA^{Glc} were the following: Cys^{15}, Cys^{40}, Cys^{128}, Cys^{276}, and Cys^{324} (Fig. 4*a*). Interestingly, these residues are located on the opposite sides of the MalK monomer but cluster together on the same side when MalK forms a dimer (Fig. 4*c*). This pattern of cross-linking is consistent with the working model presented in Fig. 3.

Finally, to confirm the orientation of EIIA^{Glc} when it is bound to MalFGK$_2$, two unique cysteine residues were introduced at positions EIIA^{Glc}-97C and EIIA^{Glc}-147C, respectively (Fig. 4*c*). We then employed a sulfhydryl-to-sulfhydryl cross-linking reagent (MTS-3-MTS; spacer arm of 5 Å) to identify the neighboring cysteine residues on MalK. This cross-link analysis showed that EIIA^{Glc}-97C is proximal to MalK-276C and MalK-324C,

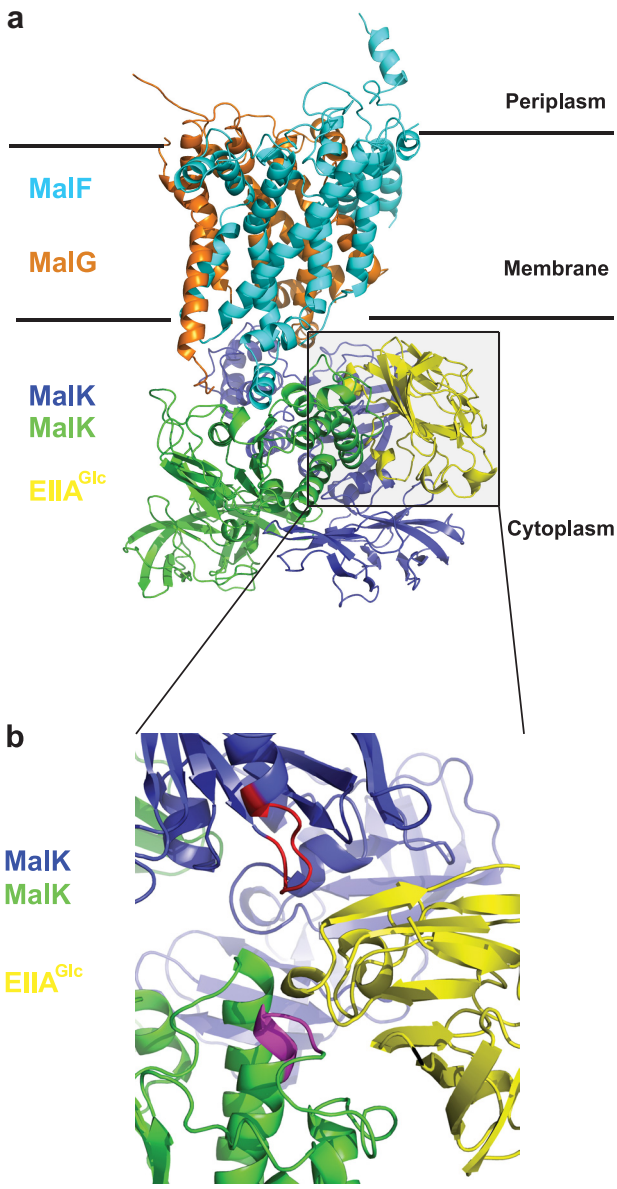

FIGURE 3. **Model of interaction between EIIA^{Glc} and MalFGK$_2$.** The model of interaction was generated with the automatic protein docking server ClusPro using the crystallography structures of EIIA^{Glc} (PDB 1F3G) and MalFGK$_2$ (PDB 3FH6). *a*, lateral view of the complex MalFGK$_2$-EIIA^{Glc} shown with the membrane plane. *Cyan*, MalF; *orange*, MalG; *blue* and *green*, MalK dimer; *yellow*, EIIA^{Glc}. Because the MalK dimer is symmetric, two EIIA^{Glc} molecules are bound per MalFGK$_2$ complex. This is not shown in the docking analysis because the computer program uses a 1:1 mode of interaction. *b*, magnified view of EIIA^{Glc} interface with MalK. The colors are the same as in *a*. In the fully closed ATP-bound conformation, the ATP molecule is contacting residues in the Walker A motif (*red*) from one MalK and the LSGGQ motif (*purple*) of the other.

whereas EIIA^{Glc}-147C is proximal to MalK-15C and MalK-40C (Fig. 4*b*). This cross-link pattern is consistent with the working model above, where each EIIA^{Glc} binds simultaneously the NBD domain of one MalK and the C-terminal domain of another MalK. Furthermore, this mode of interaction places the N-terminal tail EIIA^{Glc} in proximity to the phospholipid bilayer.

EIIA^{Glc} Does Not Inhibit the Binding of ATP to MalK—How EIIA^{Glc} inhibits the ATPase activity of MalK is unknown. EIIA^{Glc} may prevent ATP binding, ATP hydrolysis, or the release of hydrolysis products (Fig. 5). To address this question, we employed the fluorescence analog TNP-ATP. The quantum yield of TNP-ATP increases significantly upon binding to a nucleotide-binding pocket (24). However, the measurements with MalFGK$_2$ could not be reliably performed in proteoliposomes because the fluorescence emission of TNP-ATP increases in the lipid environment (data not shown). We therefore employed the MalFGK$_2$ complex reconstituted into lipid-rich nanodiscs. These lipid-rich nanodiscs reproduce the maltose transporter ATPase activity and its dependence on MalE and maltose, as in proteoliposomes (16). In addition, the amount of lipids in the particles is sufficiently low to enable fluorescence measurements. The equilibrium titrations revealed a dissociation constant (K_d) for TNP-ATP of ~9.4 μM (Fig. 5*a*). The apparent K_d for ATP, measured by competitive replacement of TNP-ATP, was estimated to be ~220 μM (Fig. 5*b*). This value is similar to the K_m derived from the ATPase measurements in lipid-rich nanodiscs and proteoliposomes (from ~200 to ~280 μM, respectively; Fig. 5*c* (25)). When these measurements were repeated in the presence of EIIA^{Glc}, no significant change in the affinity values was detected, thus indicating that EIIA^{Glc} does not inhibit the binding of ATP to the transporter (Table 1). This conclusion is consistent the docking analysis in Fig. 3*b* as the nucleotide binding site remains accessible to ATP.

EIIA^{Glc} Inhibits the Cleavage of ATP by MalK—We then tested whether EIIA^{Glc} inhibits the hydrolysis of ATP and/or the release of ADP and P$_i$. The MalFGK$_2$ complex reconstituted in lipid-rich nanodiscs was incubated with [α-^{32}P]ATP and [γ-^{32}P]ATP in the presence of MalE and maltose. After incubation, the free nucleotides were removed by centrifugal gel filtration. The nucleotides remaining bound to the transporter were detected by thin layer chromatography and autoradiography. As a control, the MalFGK$_2$ complex was incubated with sodium vanadate. With this phosphate analog, ADP remains trapped in the nucleotide-binding pocket of MalK (26). Accordingly, there was a significant increase in the amount of ADP that was co-purified with the transporter in the presence of vanadate (Fig. 5*d*, compare *lane 4* with *lane 6*). In contrast, whether EIIA^{Glc} was present or not, the amount of ADP and P$_i$ that co-purified with MalFGK$_2$ was unchanged (Fig. 5*d*, compare *lane 4* with *lane 5*). Together, these results indicate that EIIA^{Glc} does not increase or decrease the affinity of MalFGK$_2$ for ADP and P$_i$.

Finally, we assessed whether EIIA^{Glc} inhibits the ATP cleavage step by testing the ATPase activity of MalFGK$_2$ under two different conditions: (i) with MalFGK$_2$ present in 20-fold molar excess over the nucleotide, so that only a single round of ATP hydrolysis can occur; and (ii) under steady-state conditions, where the nucleotide is present in 1000-fold excess over MalFGK$_2$ so that multiple rounds of ATP hydrolysis are possible. A control experiment showed that sodium vanadate affects the cleavage of ATP only in steady-state conditions, as expected; vanadate does not inhibit the chemistry of ATP hydrolysis, but rather the release of ADP (Fig. 5*e*, compare *lane 3* with *lane 6*). In the presence of EIIA^{Glc}, however, the number of ATP molecules hydrolyzed was decreased by more than 50%, under both single and multiple turnover conditions (Fig. 5*e*). Together, these results show that the binding of EIIA^{Glc} to the

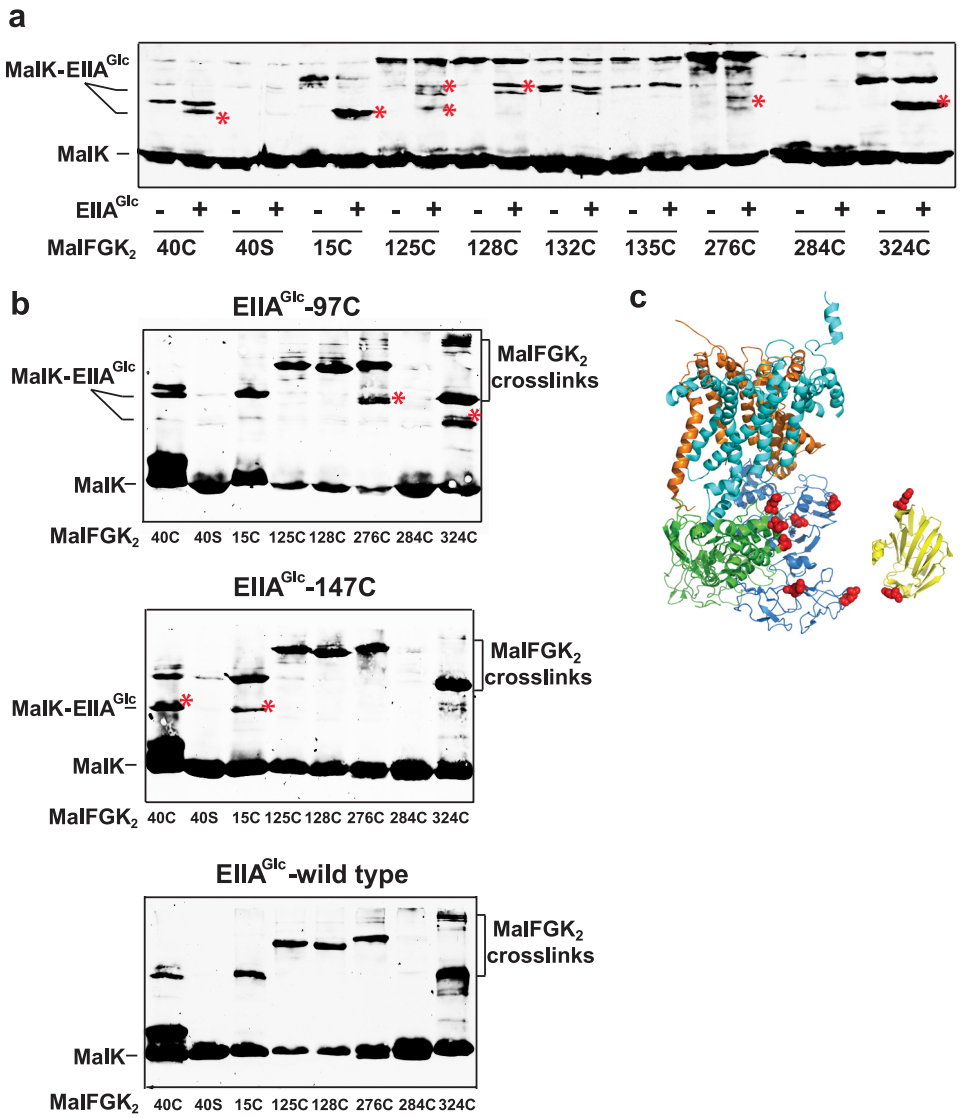

FIGURE 4. **The cross-linking analysis supports the docking analysis prediction.** *a*, the MalFGK$_2$ complex carrying the indicated cysteine residue was reconstituted in proteoliposome. The proteoliposomes (2 μM each) were incubated with wild type EIIA^{Glc} (10 μM) in the presence of the sulfhydryl- and amino-reactive cross-linker SPDP (100 μM). The reactions were stopped with Tris-HCl (100 mM, pH 8). The proteins were dissolved in sample buffer, and the cross-link products were detected by immunoblot against MalK. The cross-links corresponding to a complex between MalK and EIIA^{Glc} are annotated by a *red asterisk*. The cross-link products MalK-EIIA^{Glc} have two distinct mobilities during electrophoresis. *b*, the proteins EIIA^{Glc}-97C and EIIA^{Glc}-147C were incubated with the indicated MalFGK$_2$ proteoliposomes in the presence of sulfhydryl-reactive homobifunctional cross-linker MTS-3-MTS (100 μM, 20 min, room temperature). The reactions were stopped by *N*-ethylmaleimide (5 mM). The cross-link products were detected by immunoblot against MalK. The *red asterisk* denotes the cross-links between MalK and EIIA^{Glc}. The cross-linking pattern obtained with wild type EIIA^{Glc} is presented for comparison. *c*, the cysteine residues introduced into MalK and EIIA^{Glc} are indicated by the *red spheres*.

transporter inhibits the cleavage of ATP, and not the binding or the release of the nucleotides from MalK.

DISCUSSION

EIIA^{Glc} regulates the activity of at least 10 distinct proteins in the context of glucose uptake and catabolic repression (1, 2). Furthermore, the regulated proteins are located both in the cytosol and in the membrane and have little or no obvious structural homology with one another (3, 7). Not surprisingly therefore, the regulatory interactions of EIIA^{Glc} with these diverse proteins are generally weak and transient (6, 8, 21). This seems particularly true for the membrane permeases. *In vivo*, the inhibition of the maltose transporter requires ~5-fold more EIIA^{Glc} than the glycerol kinase (27). Because the affinity of EIIA^{Glc} for the glycerol kinase is only ~4 μM (28), it is likely that the affinity of EIIA^{Glc} for the maltose transporter is even lower. As a direct consequence, the biochemical and structural analysis of the MalFGK$_2$-EIIA^{Glc} complex is difficult, and the molecular basis of the inhibition remains obscure.

In the work reported here, we provide direct evidence that the N-terminal tail of EIIA^{Glc} together with PG lipids is essential for high affinity binding to the maltose transporter. It was previously reported that deletion of the N-terminal tail of EIIA^{Glc} relieves the inhibitory activity on the lactose and maltose transporter, but not on the cytosolic effectors (8, 9, 11, 12). It was also shown that a peptide corresponding to the N-terminal tail of EIIA^{Glc} adopts an amphipathic α-helix structure in the presence of PG lipids, but remains in a random coil with PC

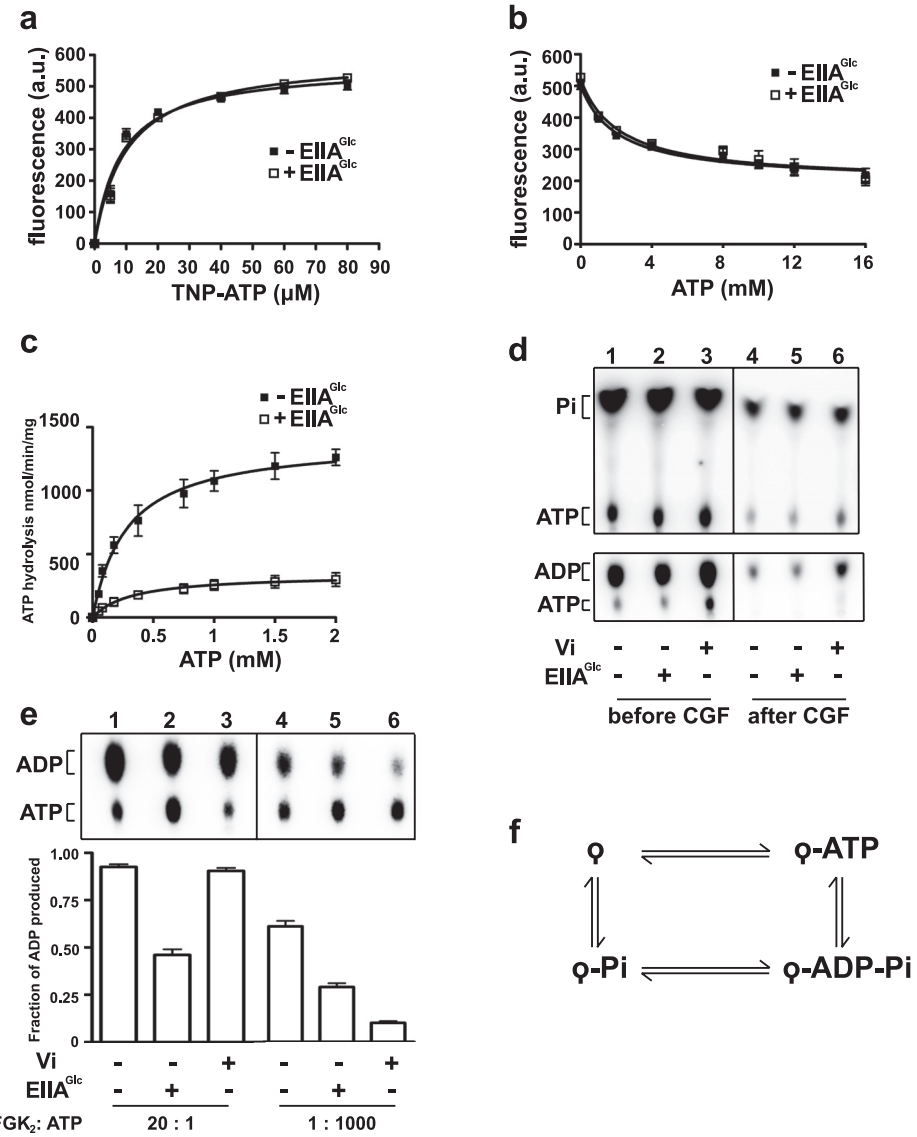

FIGURE 5. **EIIA^{Glc} inhibits the cleavage of ATP but not the binding to MalK.** *a*, equilibrium titration of MalFGK$_2$ with TNP-ATP. The MalFGK$_2$ complex reconstituted in lipid-rich nanodiscs (as in Fig. 1) was incubated with TNP-ATP (3 min, 25 °C) in the presence of MalE (10 μM), maltose (1 mM), and EIIA^{Glc} (96 μM) as indicated. The fluorescent data (mean ± S.D., $n = 3$ independent replicates) were fit to Equation 1 ("Experimental Procedures") to determine the affinity of TNP-ATP for MalK. The calculated dissociation constant (K_d) is 9.4 ± 1.2 μM in the absence of EIIA^{Glc} and 10.1 ± 1.3 μM in the presence of EIIA^{Glc}. *a. u.*, arbitrary units. *b*, equilibrium titration of MalFGK$_2$ with ATP. The MalFGK$_2$ complex reconstituted in lipid-rich nanodiscs was incubated with TNP-ATP (80 μM) in the presence of MalE (10 μM), maltose (1 mM), and EIIA^{Glc} (96 μM) as indicated. The fluorescence was measured after the addition of the indicated amount of ATP. The data (mean ± S.D., $n = 3$ independent replicates) were fit to Equations 2 and 3 as described under "Experimental Procedures." The calculated apparent dissociation constant for ATP ($K_{d,app}$) is 222 ± 31 μM in the absence of EIIA^{Glc} and 236 ± 29 μM in the presence of EIIA^{Glc} (Table 1). *c*, rate of ATP hydrolysis. The rate was determined with the lipid-rich MalFGK$_2$ nanodiscs (2 μM) at the indicated ATP concentration, in the presence of MalE (10 μM), maltose (1 mM), and EIIA^{Glc} (96 μM). The data (mean ± S.D., $n = 3$ independent replicates) were fit to the Michaelis-Menten equation to determine the K_m. The calculated Michaelis-Menten constant (K_m) is 279 ± 47 μM in the absence of EIIA^{Glc} and 294 ± 64 μM in the presence of EIIA^{Glc}. These values are comparable with those determined in *b*. The K_m for ATP when MalFGK$_2$ in reconstituted in proteoliposome is ~200 μM (25). *d*, effect of EIIA^{Glc} on the release of ADP and P$_i$. The lipid-rich MalFGK$_2$ nanodiscs (20 μM), MalE (75 μM), and maltose (1 mM) were incubated for 10 min at room temperature with 300 μM [α-^{32}P]ATP (*lower panel*) or 300 μM [γ-^{32}P]ATP (*upper panel*), with or without EIIA^{Glc} (96 μM) as specified. The control experiment with 200 μM vanadate (*Vi*) was performed in parallel. The total amount of ADP and P$_i$ produced during the reaction was determined by TLC before centrifugal gel filtration (*CGF*). The total amount of ADP and P$_i$ remaining bound to the transporter was determined by TLC after centrifugal gel filtration. The TLC plate was developed in 0.3 M potassium phosphate, pH 3.4, followed by autoradiography analysis. *e*, effect of EIIA^{Glc} on ATP hydrolysis in single and multiple turnovers. The lipid-rich MalFGK$_2$ nanodiscs (*left panel*, 20 μM; *right panel*, 1 μM) were incubated with MalE (75 μM) and maltose (1 mM) at room temperature with [α-^{32}P]ATP (*left panel*, 1 μM ATP for 1 min; *right panel*, 1 mM ATP for 10 min), in the presence of EIIA^{Glc} (96 μM) or vanadate (200 μM) as indicated. The reactions were stopped by the addition of ice-cold EDTA (20 mM) and proteinase K (1 mg/ml). Samples were analyzed by TLC and autoradiography. The radioactive spots (mean ± S.D., $n = 3$ independent replicates) were quantified by densitometry to determine the fraction of ADP produced. *f*, the ATPase cycle is a succession of four chemical steps: ATP binding, ATP cleavage, phosphate dissociation, and ADP dissociation. MalFGK$_2$ is denoted as a *tailed circle*.

lipids (8, 13). Our work thus links these observations together and demonstrates the importance of acidic lipids for directing EIIA^{Glc} to the maltose transporter. We propose that the affinity of EIIA^{Glc} for acidic lipids, combined with a restricted diffusion of the protein bound to the lipid bilayer, serves to increase the otherwise low affinity interaction of EIIA^{Glc} with the maltose transporter. Accordingly, a previous study indicated that EIIA^{Glc} weakly inhibits the ATPase activity of the MalK subunit

TABLE 1
Equilibrium constants of TNP-ATP and ATP for the maltose transporter MalFGK$_2$

	K_d of TNP-ATP	$K_{d,app}$ of ATP	K_m of ATP
	μM	μM	μM
MalFGK$_2$	9.4 ± 1.2	222 ± 31	279 ± 47
MalFGK$_2$ + EIIA^{Glc}	10.1 ± 1.3	236 ± 29	294 ± 64

in solution (29). It is tempting to speculate that the membrane lipid composition might be an important parameter for the regulation of MalFGK$_2$ by EIIA^{Glc}. In this context, we recently reported that the length of the lipid acyl chain is a strong determinant of the maltose transporter activity (16).

In addition to its targeting function, the N-terminal tail probably allows the optimal positioning of the C-terminal inhibitory domain of EIIA^{Glc} on the transporter catalytic site. In the absence of co-crystals between EIIA^{Glc} and MalFGK$_2$, we employed a molecular docking method to identify potential binding surfaces. We then introduced a series of unique cysteine residues to perform amine-to-sulfhydryl and sulfhydryl-to-sulfhydryl cross-linking analysis. By combining these approaches, we were able to identify a binding interface comprising the NBD domain and C-terminal domain on the MalK dimer and the β-strands 5 and 7 on EIIA^{Glc} (Fig. 4). In our working model (Fig. 3), the N-terminal tail of EIIA^{Glc} is facing the lipid membrane, whereas the globular domain of EIIA^{Glc} spans the MalK dimer interface, in direct contact with the NBD and C-terminal regulatory domains. Because the MalK dimer is symmetric, two EIIA^{Glc} molecules are bound per MalFGK$_2$ complex. This model is consistent with the cooperative inhibition we observe (Fig. 1*c*) and the location of the mutations that cause resistance to EIIA^{Glc} (21–23). These mutations (*i.e.* A124T, F241I, G278P, G284S, E119K, R228C, G302D, and S322F) are located on opposite sides on the monomer, but on the same side when MalK forms a dimer. Interestingly, in our working model, the tip of the regulatory domain on MalK remains accessible for binding and segregation of the transcriptional activator MalT (23, 30). Should this be the case, the action of EIIA^{Glc} and MalT would be complementary, meaning that the cell would be able to inhibit maltose transport and keep *mal* gene expression to basal level by acting on the same complex simultaneously.

How EIIA^{Glc} inhibits the activity of the transporter was an important unanswered question. The dissection of the MalFGK$_2$ ATPase cycle allows us to conclude that EIIA^{Glc} inhibits the cleavage of ATP by MalK, not the binding of the molecule or the release of the hydrolysis products. Because the binding of ATP leads to the closure of the MalK dimer, and because the closure of the MalK dimer is necessary for ATP hydrolysis (31), we conclude that EIIA^{Glc} interferes at the closure step. In the magnified view of the modeled EIIA^{Glc}-MalFGK$_2$ complex, part of EIIA^{Glc} is inserted between the NBD domains of MalK (Fig. 3*b*). Blocking the closure of the MalK dimer would also stabilize the MalFG membrane domain in its inward-facing conformation (*i.e.* transporter closed on the periplasmic side). Because MalE binds with a high affinity to only the outward-facing conformation (15), it is predicted that EIIA^{Glc} also prevents the binding of MalE to the transporter.

Finally, how the phosphorylation of one residue (*i.e.* His^{90}) prevents the action of EIIA^{Glc} on the maltose transporter is another important question. The co-crystal structure of EIIA^{Glc} with the glycerol kinase (Protein Data Bank code 1GLA) indicates that the phosphorylation of His^{90} causes charge repulsion with the residue Glu^{478} in the glycerol kinase, thereby reducing the interaction and inhibitory capacity of EIIA^{Glc} (5, 7). A similar mechanism is perhaps occurring for the maltose transporter. In our working model, His^{90} on EIIA^{Glc} is within ~10 Å distance to Asp^{119} on MalK. Further biochemical and structural analysis will tell how phosphorylation of a single residue can suppress the inhibitory activity of EIIA^{Glc} on the maltose transporter.

Acknowledgments—We thank Dr. Amy Davidson, Purdue University, for the generous gift of MalK antibodies and Sung Hoon Choi for valuable help in making constructs.

REFERENCES

1. Görke, B., and Stülke, J. (2008) Carbon catabolite repression in bacteria: many ways to make the most out of nutrients. *Nat. Rev. Microbiol.* **6,** 613–624
2. Postma, P. W., Lengeler, J. W., and Jacobson, G. R. (1993) Phosphoenolpyruvate:carbohydrate phosphotransferase systems of bacteria. *Microbiol. Rev.* **57,** 543–594
3. Deutscher, J., Francke, C., and Postma, P. W. (2006) How phosphotransferase system-related protein phosphorylation regulates carbohydrate metabolism in bacteria. *Microbiol. Mol. Biol. Rev.* **70,** 939–1031
4. Worthylake, D., Meadow, N. D., Roseman, S., Liao, D. I., Herzberg, O., and Remington, S. J. (1991) Three-dimensional structure of the *Escherichia coli* phosphocarrier protein IIIglc. *Proc. Natl. Acad. Sci. U.S.A.* **88,** 10382–10386
5. Hurley, J. H., Faber, H. R., Worthylake, D., Meadow, N. D., Roseman, S., Pettigrew, D. W., and Remington, S. J. (1993) Structure of the regulatory complex of *Escherichia coli* IIIGlc with glycerol kinase. *Science* **259,** 673–677
6. Cai, M., Williams, D. C., Jr., Wang, G., Lee, B. R., Peterkofsky, A., and Clore, G. M. (2003) Solution structure of the phosphoryl transfer complex between the signal-transducing protein IIA^{Glucose} and the cytoplasmic domain of the glucose transporter IICB^{Glucose} of the *Escherichia coli* glucose phosphotransferase system. *J. Biol. Chem.* **278,** 25191–25206
7. Wang, G., Louis, J. M., Sondej, M., Seok, Y. J., Peterkofsky, A., and Clore, G. M. (2000) Solution structure of the phosphoryl transfer complex between the signal transducing proteins HPr and IIA^{Glucose} of the *Escherichia coli* phosphoenolpyruvate:sugar phosphotransferase system. *EMBO J.* **19,** 5635–5649
8. Wang, G., Peterkofsky, A., and Clore, G. M. (2000) A novel membrane anchor function for the N-terminal amphipathic sequence of the signal-transducing protein IIA^{Glucose} of the *Escherichia coli* phosphotransferase system. *J. Biol. Chem.* **275,** 39811–39814
9. Blüschke, B., Volkmer-Engert, R., and Schneider, E. (2006) Topography of the surface of the signal-transducing protein EIIA^{Glc} that interacts with the MalK subunits of the maltose ATP-binding cassette transporter (MalFGK$_2$) of *Salmonella typhimurium*. *J. Biol. Chem.* **281,** 12833–12840
10. Sondej, M., Seok, Y. J., Badawi, P., Koo, B. M., Nam, T. W., and Peterkofsky, A. (2000) Topography of the surface of the *Escherichia coli* phosphotransferase system protein enzyme IIA^{glc} that interacts with lactose permease. *Biochemistry* **39,** 2931–2939
11. Misko, T. P., Mitchell, W. J., Meadow, N. D., and Roseman, S. (1987) Sugar transport by the bacterial phosphotransferase system: reconstitution of inducer exclusion in *Salmonella typhimurium* membrane vesicles. *J. Biol. Chem.* **262,** 16261–16266
12. Meadow, N. D., and Roseman, S. (1982) Sugar transport by the bacterial phosphotransferase system: isolation and characterization of a glucose-

specific phosphocarrier protein (III^{Glc}) from *Salmonella typhimurium*. *J. Biol. Chem.* **257,** 14526–14537
13. Wang, G., Keifer, P. A., and Peterkofsky, A. (2003) Solution structure of the N-terminal amphitropic domain of *Escherichia coli* glucose-specific enzyme IIA in membrane-mimetic micelles. *Protein Sci.* **12,** 1087–1096
14. Bao, H., and Duong, F. (2012) Discovery of an auto-regulation mechanism for the maltose ABC transporter MalFGK$_2$. *PLoS One* **7,** e34836
15. Bao, H., and Duong, F. (2013) ATP alone triggers the outward facing conformation of the maltose ATP-binding cassette transporter. *J. Biol. Chem.* **288,** 3439–3448
16. Bao, H., Dalal, K., Wang, V., Rouiller, I., and Duong, F. (2013) The maltose ABC transporter: Action of membrane lipids on the transporter stability, coupling, and ATPase activity. *Biochim. Biophys. Acta* **1828,** 1723–1730
17. Sharma, S., Davis, J. A., Ayvaz, T., Traxler, B., and Davidson, A. L. (2005) Functional reassembly of the *Escherichia coli* maltose transporter following purification of a MalF-MalG subassembly. *J. Bacteriol.* **187,** 2908–2911
18. Kozakov, D., Hall, D. R., Beglov, D., Brenke, R., Comeau, S. R., Shen, Y., Li, K., Zheng, J., Vakili, P., Paschalidis, I.Ch., and Vajda, S. (2010) Achieving reliability and high accuracy in automated protein docking: ClusPro, PIPER, SDU, and stability analysis in CAPRI rounds 13–19. *Proteins* **78,** 3124–3130
19. Oldham, M. L., Khare, D., Quiocho, F. A., Davidson, A. L., and Chen, J. (2007) Crystal structure of a catalytic intermediate of the maltose transporter. *Nature* **450,** 515–521
20. Khare, D., Oldham, M. L., Orelle, C., Davidson, A. L., and Chen, J. (2009) Alternating access in maltose transporter mediated by rigid-body rotations. *Mol. Cell* **33,** 528–536
21. Dean, D. A., Reizer, J., Nikaido, H., and Saier, M. H., Jr. (1990) Regulation of the maltose transport system of *Escherichia coli* by the glucose-specific enzyme III of the phosphoenolpyruvate-sugar phosphotransferase system: characterization of inducer exclusion-resistant mutants and reconstitution of inducer exclusion in proteoliposomes. *J. Biol. Chem.* **265,** 21005–21010
22. Kühnau, S., Reyes, M., Sievertsen, A., Shuman, H. A., and Boos, W. (1991) The activities of the *Escherichia coli* MalK protein in maltose transport, regulation, and inducer exclusion can be separated by mutations. *J. Bacteriol.* **173,** 2180–2186
23. Böhm, A., Diez, J., Diederichs, K., Welte, W., and Boos, W. (2002) Structural model of MalK, the ABC subunit of the maltose transporter of *Escherichia coli*: implications for *mal* gene regulation, inducer exclusion, and subunit assembly. *J. Biol. Chem.* **277,** 3708–3717
24. Poolman, B., Doeven, M. K., Geertsma, E. R., Biemans-Oldehinkel, E., Konings, W. N., and Rees, D. C. (2005) Functional analysis of detergent-solubilized and membrane-reconstituted ATP-binding cassette transporters. *Methods Enzymol.* **400,** 429–459
25. Davidson, A. L., Laghaeian, S. S., and Mannering, D. E. (1996) The maltose transport system of *Escherichia coli* displays positive cooperativity in ATP hydrolysis. *J. Biol. Chem.* **271,** 4858–4863
26. Chen, J., Sharma, S., Quiocho, F. A., and Davidson, A. L. (2001) Trapping the transition state of an ATP-binding cassette transporter: evidence for a concerted mechanism of maltose transport. *Proc. Natl. Acad. Sci. U.S.A.* **98,** 1525–1530
27. van der Vlag, J., van Dam, K., and Postma, P. W. (1994) Quantification of the regulation of glycerol and maltose metabolism by IIAGlc of the phosphoenolpyruvate-dependent glucose phosphotransferase system in *Salmonella typhimurium*. *J. Bacteriol.* **176,** 3518–3526
28. Novotny, M. J., Frederickson, W. L., Waygood, E. B., and Saier, M. H., Jr. (1985) Allosteric regulation of glycerol kinase by enzyme IIIglc of the phosphotransferase system in *Escherichia coli* and *Salmonella typhimurium*. *J. Bacteriol.* **162,** 810–816
29. Landmesser, H., Stein, A., Blüschke, B., Brinkmann, M., Hunke, S., and Schneider, E. (2002) Large-scale purification, dissociation and functional reassembly of the maltose ATP-binding cassette transporter (MalFGK$_2$) of *Salmonella typhimurium*. *Biochim. Biophys. Acta* **1565,** 64–72
30. Richet, E., Davidson, A. L., and Joly, N. (2012) The ABC transporter MalFGK$_2$ sequesters the MalT transcription factor at the membrane in the absence of cognate substrate. *Mol. Microbiol.* **85,** 632–647
31. Chen, J., Lu, G., Lin, J., Davidson, A. L., and Quiocho, F. A. (2003) A tweezers-like motion of the ATP-binding cassette dimer in an ABC transport cycle. *Mol. Cell* **12,** 651–661